



Virtual Special Issue Ocean Surface Waves

Ocean surface waves in Hurricane Ike (2008) and Superstorm Sandy (2012): Coupled model predictions and observations



Shuyi S. Chen*, Milan Curcic

Rosenstiel School of Marine and Atmospheric Science, University of Miami, 4600 Rickenbacker Causeway, Miami, FL 33149, United States

ARTICLE INFO

Article history:

Received 6 February 2015

Revised 10 August 2015

Accepted 27 August 2015

Available online 3 September 2015

Keywords:

Ocean surface waves

Hurricanes

Coupled atmosphere-wave-ocean modeling and prediction

Surface wave observations

ABSTRACT

Forecasting hurricane impacts of extreme winds and flooding requires accurate prediction of hurricane structure and storm-induced ocean surface waves days in advance. The waves are complex, especially near landfall when the hurricane winds and water depth varies significantly and the surface waves refract, shoal and dissipate. In this study, we examine the spatial structure, magnitude, and directional spectrum of hurricane-induced ocean waves using a high resolution, fully coupled atmosphere-wave-ocean model and observations. The coupled model predictions of ocean surface waves in Hurricane Ike (2008) over the Gulf of Mexico and Superstorm Sandy (2012) in the northeastern Atlantic and coastal region are evaluated with the NDBC buoy and satellite altimeter observations. Although there are characteristics that are general to ocean waves in both hurricanes as documented in previous studies, wave fields in Ike and Sandy possess unique properties due mostly to the distinct wind fields and coastal bathymetry in the two storms. Several processes are found to significantly modulate hurricane surface waves near landfall. First, the phase speed and group velocities decrease as the waves become shorter and steeper in shallow water, effectively increasing surface roughness and wind stress. Second, the bottom-induced refraction acts to turn the waves toward the coast, increasing the misalignment between the wind and waves. Third, as the hurricane translates over land, the left side of the storm center is characterized by offshore winds over very short fetch, which opposes incoming swell. Landfalling hurricanes produce broader wave spectra overall than that of the open ocean. The front-left quadrant is most complex, where the combination of windsea, swell propagating against the wind, increasing wind-wave stress, and interaction with the coastal topography requires a fully coupled model to meet these challenges in hurricane wave and surge prediction.

© 2015 Published by Elsevier Ltd.

1. Introduction

Ocean surface waves are essential in assessing hurricane impact on marine environment and storm surge over the hurricane-prone regions of the Gulf of Mexico and US Atlantic Seaboard. Hurricane impacts are mostly felt at landfall, which are most challenging for accurate model forecasts of extreme winds, rain, waves, storm surge, and inland flooding near the coast. The totality of these hurricane impacts needs be represented in fully coupled atmosphere-wave-ocean-land prediction models. Ocean surface waves played an important role in the record-breaking storm surge in New York during Superstorm Sandy (2012) at landfall when the water level were elevated by the wave set up as described in an observational study by

[Hsu \(2013\)](#). Hurricane wave “forecasting” has traditionally been done using uncoupled surface wave models forced by wind fields from either wind analysis products like the H*WIND ([Powell et al., 1998](#)) in a hindcast mode (e.g., [Hope et al., 2013](#)) or the operational atmospheric models as summarized in [Alves et al. \(2015\)](#). These approaches assume that the surface winds are not affected by the waves, which is unphysical. Furthermore, hindcast models often uses surface wind analysis field based on observations, which is fundamentally different than coupled prediction models.

Studies using coupled atmosphere-wave-ocean prediction models have shown the importance of wind-wave coupling on spatial distribution of surface waves in Hurricane Frances (2004) ([Chen et al., 2007, 2013](#)) and ocean currents and wave-current coupling on surface waves in Hurricane Ivan (2004) ([Smith et al., 2013](#)). More importantly, these fully coupled prediction models are capable of predicting coherent wind, rain, wave, and current fields in hurricanes several days in advance. Hurricane-induced waves are sensitive to

* Corresponding author. Tel.: +1 305 479 6551.

E-mail address: schen@rsmas.miami.edu (S.S. Chen).

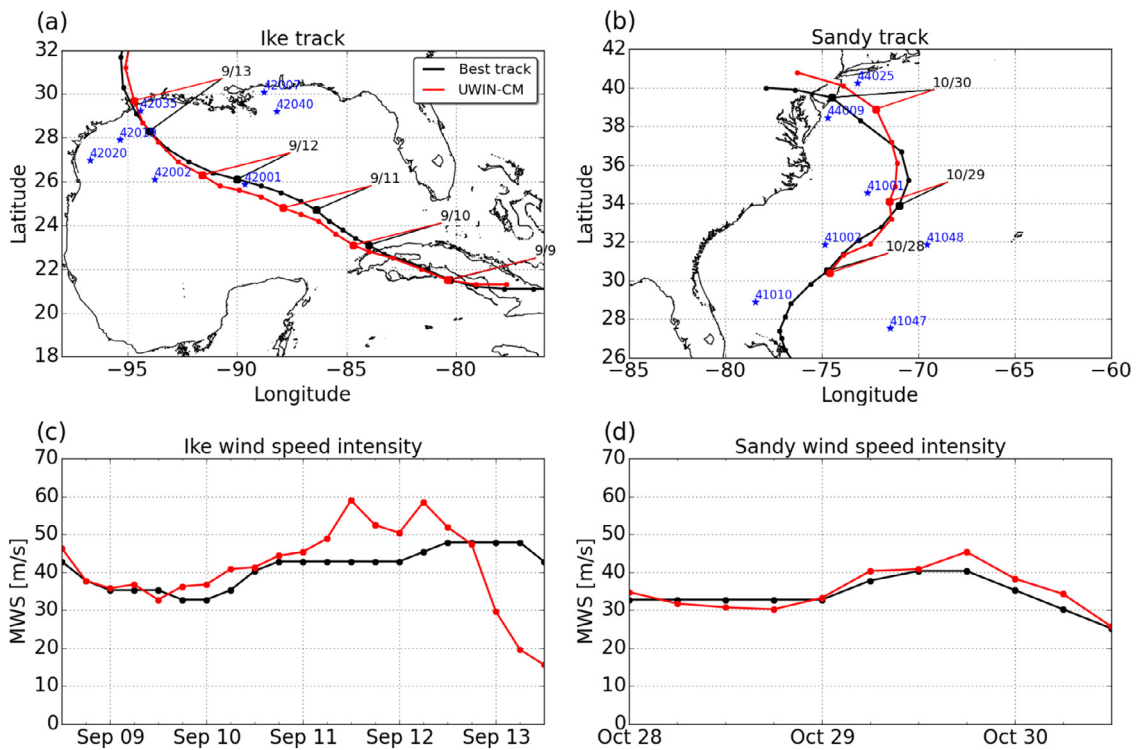


Fig. 1. The NHC best track and UWIN-CM modeled tracks and intensities of Hurricanes Ike from 8 to 13 September 2008 (a and c) and Superstorm Sandy from 28 to 30 October 2012 (b and d). The locations of NDBC buoys used in this study are shown in (a) and (b).

winds varying spatially and in time in a moving storm and have different characteristics in the open ocean and near landfall as shown by observations (Wright et al., 2001; Walsh et al., 2002). As a storm approaches the land, the wind and wave fields become more complex, in part due to the coastal land-sea features including topography and bathymetry. Surface waves refract, shoal, and dissipate in shallow waters, which can affect surface winds, currents, the mean sea level. In this study, we examine the spatial structure, magnitude, and directional spectrum of hurricane-induced ocean waves from open ocean to at landfall using a high resolution, fully coupled atmosphere-wave-ocean model and in situ and remote sensing observations.

We first provide a description of the coupled atmosphere-wave-ocean modeling system in Section 2. The coupled model simulation of Hurricane Ike and prediction of Superstorm Sandy as well as storm-induced waves are compared with observations in Sections 3 and 4. Sections 5 and 6 examine the spatial and temporal variations of directional wave spectrum and mean wave properties in the open ocean and near landfall, respectively. A summary and conclusions are given in Section 7.

2. Coupled model

A key feature of the coupled modeling system is a unified air-sea interface, namely the Unified Wave INterface (UWIN). It is designed to be flexible in a multi-model system and portable for transition to the next generation fully coupled regional and global atmosphere-wave-ocean-land models. It couples the atmosphere, wave, and ocean model components using the Earth System Modeling Framework (ESMF, Hill et al., 2004). UWIN has been implemented in the Coupled Model (UWIN-CM) developed at the University of Miami, which consists of the atmosphere, wave, and ocean model components.

2.1. Atmosphere model

The atmospheric model in UWIN-CM is the Weather Research and Forecasting (WRF) model V3.5 with Advanced Research WRF (ARW) dynamical core (Skamarock et al., 2008). WRF is a non-hydrostatic atmospheric model with a large number of model physics options and a storm-following, moving nest capability for hurricane forecasting. The outermost domain is from 55.0 to 103.0W in longitude and 7.0–45.0N in latitude with a 12 km horizontal grid spacing and 36 vertical levels. There are two vortex-following inner nests of $2000 \times 2000 \text{ km}^2$ and $440 \times 440 \text{ km}^2$ with 4 and 1.3 km grid spacing, respectively. The surface layer is based on the Monin–Obukhov theory and boundary layer parameterization is the Yonsei University scheme (YSU, Hong et al., 2006). The cloud microphysics is the single-moment five-species scheme WSM5 (Hong et al., 2004), which is used on the two inner nested domains without cumulus parameterization. The Kain–Fritsch cumulus parameterization is used only on the 12 km domain (Kain and Fritsch, 1993) in addition to WSM5.

2.2. Ocean surface wave model

The ocean surface wave model in UWIN-CM is the University of Miami Wave Model (UMWM) V1.1.0 (Donelan et al., 2012). It is a spectral ocean wave model that predicts wave energy spectra and the atmosphere and ocean momentum fluxes based on winds and ocean currents. UMWM can be initialized either from existing wave states from a global wave model or a calm state. The wave model has the same domain as the WRF outer domain. It is configured with 4-km grid spacing in this study. The wave energy spectrum is represented by 36 directional bins and 37 frequency bins in the range from 0.0313 Hz to 2.0 Hz.

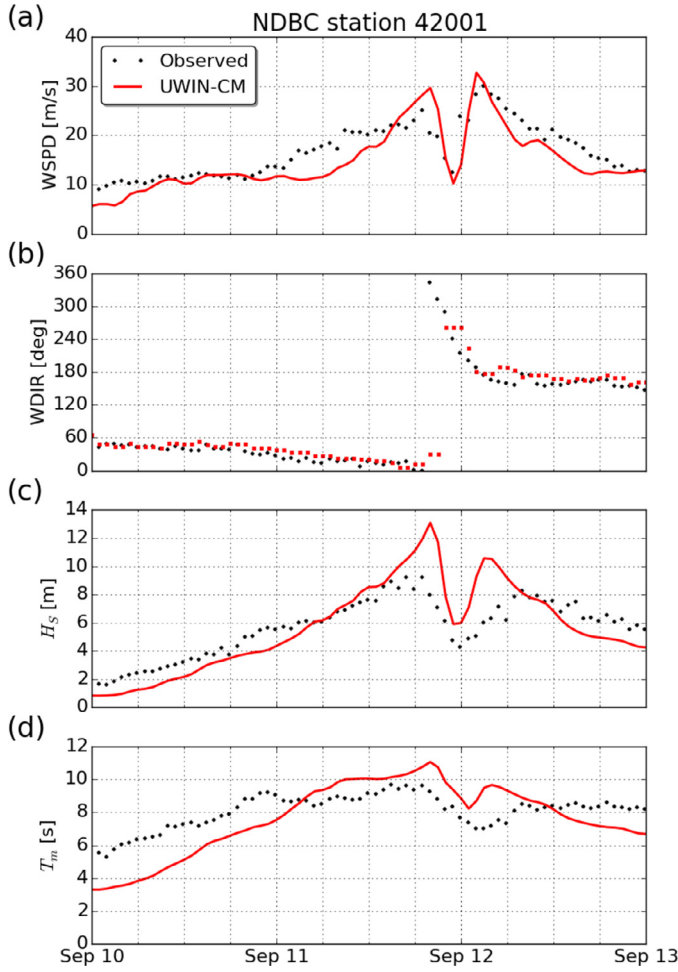


Fig. 2. Comparison of UWIN-CM results with NDBC buoy 42001 measurements of (a) wind speed and (b) direction at 5 m height, (c) significant wave height (H_s), and (d) mean wave period (T_m), in Hurricane Ike (2008). The model fields have been adjusted to account for the track error in storm center position.

2.3. Ocean circulation model

The ocean circulation model in UWIN-CM is the HYbrid Coordinate Ocean Model (HYCOM) V2.2.34 (Wallcraft et al., 2009). It is a three-dimensional hydrostatic ocean model with a hybrid vertical coordinate: z-level in shallow waters, terrain-following coordinate in intermediate waters, and isopycnal (constant density) in deep waters. In this study, we use the non-local K -profile vertical mixing scheme by Large et al. (1994). HYCOM domain covers the region of the WRF outer domain. It is configured with 0.04° horizontal grid spacing (varying from ~ 3.8 to 4.4 km from north-south of the model domain) and 32 vertical levels.

2.4. Atmosphere-wave-ocean coupling

The UWIN handles the coupling between model components. It contains the coupling physics and a common exchange grid that is used for interpolation and calculation of air-sea exchange fields from the component models. WRF passes the wind profile and air density to the wave model, and radiative and heat fluxes and precipitation rate to the ocean circulation model. UMWM passes vectorial atmosphere stress to the atmosphere model, and vectorial ocean stress to the ocean circulation model. HYCOM passes sea surface temperature (SST) to the atmosphere model and surface current field and water

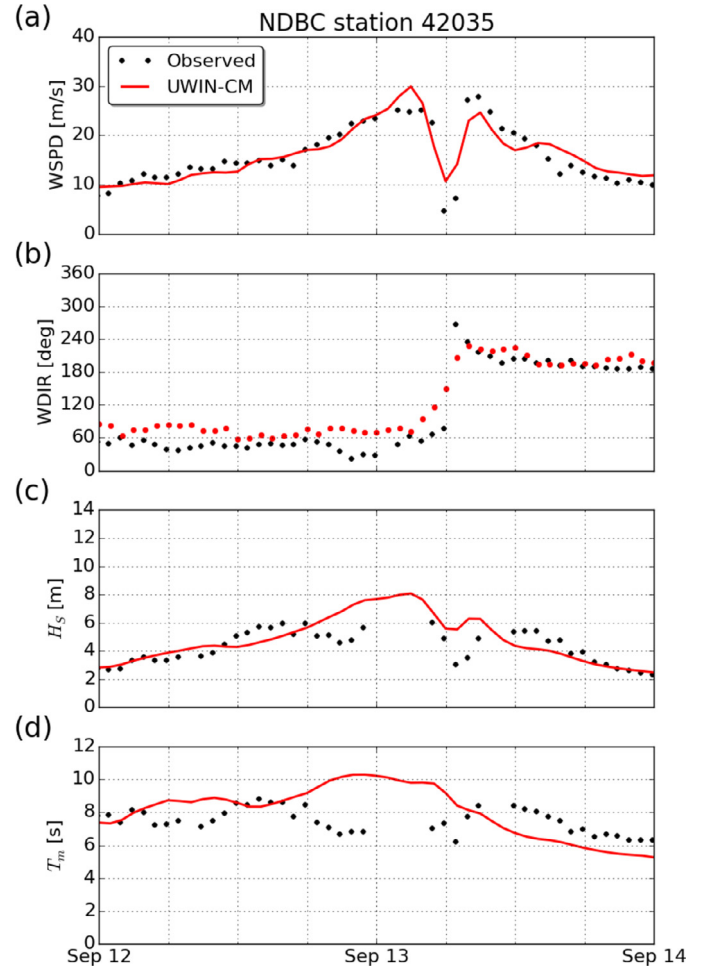


Fig. 3. Same as in Fig. 2, except for NDBC buoy 42035, located in shallow water near the Texas coast (see Fig. 1a).

density to the wave model. All fields are interpolated to the exchange grid and are co-located in discrete time. In the current model configuration, fields from WRF and UMWM are exchanged every 60 s, whereas HYCOM fields are exchanged every 120 s.

2.5. Initial and lateral boundary conditions

The WRF model initial and lateral boundary conditions were from the National Center for Environmental Prediction (NCEP) Global Forecasting System (GFS) six-hourly analysis 0.5° horizontal resolution in the case of Hurricane Ike (2008) and the GFS realtime forecast fields for Superstorm Sandy (2012). We refer to model simulation when the GFS analysis fields were used and prediction when the GFS forecast fields were used. The initial and boundary conditions for the ocean model are provided by the global, data assimilated, 0.08° horizontal resolution daily HYCOM fields. The UWIN-CM simulation of Hurricane Ike was initialized at 1200 UTC on 8 September 2008. The UWIN-CM forecast of Superstorm Sandy was initialized at 0000 UTC on 27 October 2012.

3. Hurricane Ike and Superstorm Sandy

To better understand the variability of hurricane-induced ocean surface waves due to variations of wind field, coastline, and bathymetry, two distinct hurricanes are selected for this study.

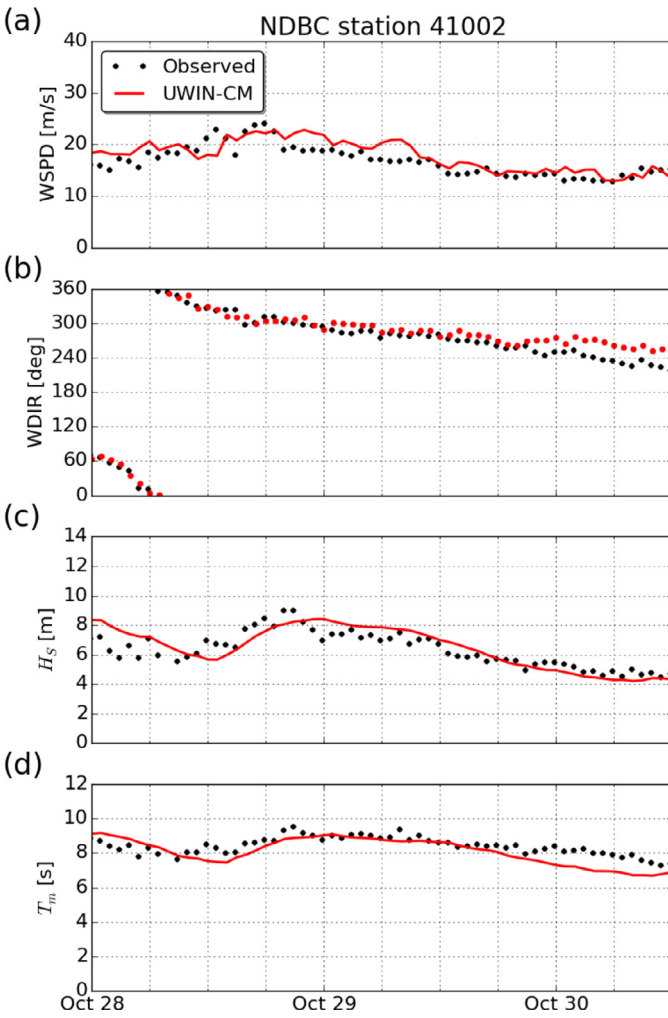


Fig. 4. Same as in Fig. 2, except for NDBC buoy 41002, located on the left side of Sandy's track in 2012 (Fig. 1d).

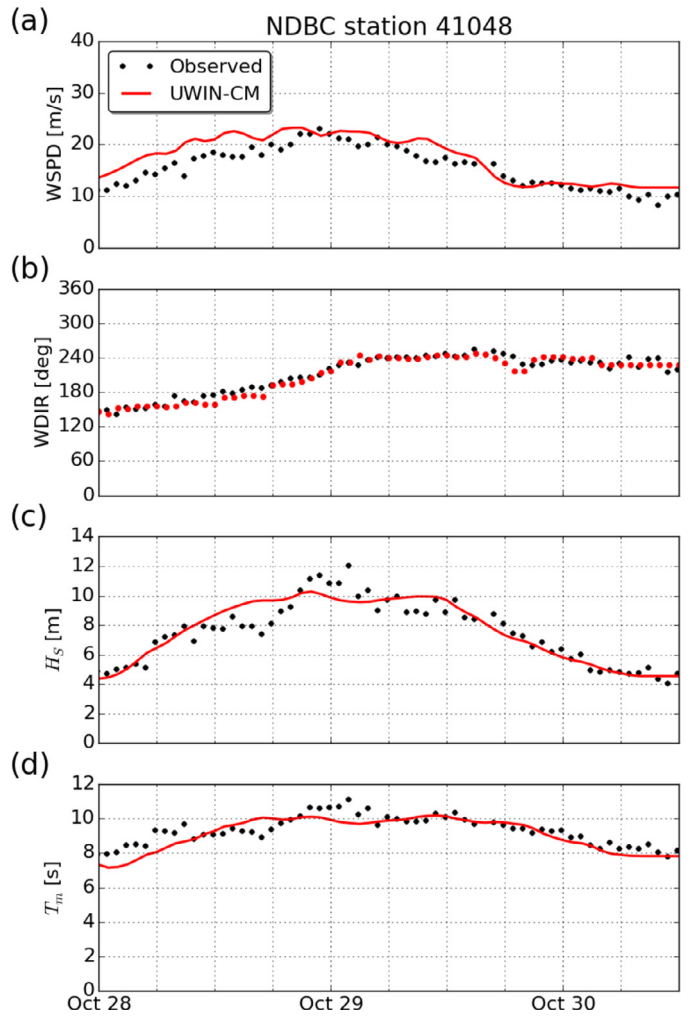


Fig. 5. Same as in Fig. 2, except for NDBC buoy 41048, located on the right side of Sandy's track (Fig. 1b).

Hurricane Ike was a Category 3 major hurricane that propagated through the Gulf of Mexico and made the landfall near Galveston, Texas, on 13 September 2008.

Superstorm Sandy formed as a tropical storm in the Caribbean Sea on 23 October 2012 and later intensified into a hurricane of the western Atlantic Ocean. It interacted with a strong mid-latitude system and became a “superstorm” that made landfall in the New Jersey and New York coasts on 30 October 2012.

The coupled model simulated and predicted tracks and maximum wind speeds (MWS) of Ike and Sandy are compared with the National Hurricane Center (NHC) Best Track (BT) estimates (Fig. 1), respectively. In Ike, the simulated track is in a good agreement with BT, except for a faster translation speed than BT. The model simulated storm made landfall at the Galveston Bay about 11 h earlier than the observation (Fig. 1a). The model simulated MWS is higher than the BT estimates on 11–12 September (Fig. 1c). The simulated MWS decreases rapidly at ~1800 UTC on 12 September at landfall, which is earlier than observed. In Sandy, the model predicted track and intensity were relatively accurate compared with the BT estimates (Fig. 1b and d). The predicted track has a northward bias from 28 to 29 October (Fig. 1b) and slightly slower translation speed, which makes landfall 6 h later compared to BT estimate, and approximately 60 km to the North. The MWS is slightly over-predicted on 29 October (Fig. 1d).

4. Wind and wave observations and model verification

Hurricane wind and wave vary greatly within each storm and evolve in time. The waves were not only affected by the maximum wind speed, but also by the size and translation speed of the hurricane among other factors. The impact of hurricane-induced waves varies spatially and temporally from location to location. It is imperative that we evaluate the coupled model results against the measurements from both the National Data Buoy Center's (NDBC) buoys and the satellite altimeter data from Jason-1 and Jason-2.

We first examine the wind speed and direction, significant wave height (H_s), and zero-crossing mean wave period measured and modeled at various NDBC buoy locations. The NDBC buoys have a frequency range from 0.02 to 0.485 Hz. The wave instrumentation and data acquisition of the NDBC buoys are described by Earle (1996). A total of 14 NDBC buoys are included for the model verification, seven in Hurricane Ike (Fig. 1a) and seven in Superstorm Sandy (Fig. 1b). Here we focus on the variation of hurricane-induced winds and waves along the storm track in Ike and in the right and left sides of the storm track in Sandy.

The NDBC buoys 42001 and 42035 are located in the deep and shallow waters along the track of Ike, respectively. Both stations experienced the passage of the eye and high winds and waves associated with the eyewall (Figs. 2 and 3). The coupled model captured the

Table 1

Model verification statistics comparing the UWIN-CM simulated and NDBC buoy measured wind speed at 5-m height (U_5), significant wave height (H_s), and zero-crossing mean wave period (T_m) at buoys 42001–42040 in Hurricane Ike (2008), and 41001–44025 in Superstorm Sandy (2012). Model bias, mean absolute error (MAE), and root mean squared error (ε_{rms}) are listed by variable (unit) and value (percentage relative to the mean observed quantity).

NDBC station #	Variable	Bias	MAE	ε_{rms}
Ike (2008): 42001	U_5 (m/s)	-2.01 (-12%)	3.27 (19%)	4.26 (25%)
	H_s (m)	0.01 (0%)	1.32 (23%)	1.81 (32%)
	T_m (s)	-0.44 (-5%)	1.39 (17%)	1.55 (19%)
42002	U_5 (m/s)	-1.12 (-8%)	1.78 (12%)	2.42 (17%)
	H_s (m)	0.45 (10%)	0.85 (20%)	1.02 (24%)
	T_m (s)	0.26 (3%)	1.10 (15%)	1.25 (17%)
42007	U_5 (m/s)	-0.58 (-5%)	1.05 (8%)	1.21 (10%)
	H_s (m)	-0.39 (-12%)	0.43 (13%)	0.49 (15%)
	T_m (s)	-1.14 (-16%)	1.15 (16%)	1.25 (18%)
42019	U_5 (m/s)	-0.73 (-5%)	1.26 (9%)	1.47 (11%)
	H_s (m)	0.15 (4%)	0.55 (15%)	0.64 (17%)
	T_m (s)	-0.23 (-3%)	1.31 (18%)	1.41 (19%)
42020	U_5 (m/s)	-0.76 (-9%)	1.78 (20%)	2.21 (25%)
	H_s (m)	-1.04 (-27%)	1.09 (29%)	1.33 (35%)
	T_m (s)	-1.30 (-16%)	1.61 (20%)	1.93 (23%)
42035	U_5 (m/s)	0.16 (1%)	1.83 (11%)	2.23 (14%)
	H_s (m)	0.11 (1%)	0.73 (17%)	1.02 (24%)
	T_m (s)	0.27 (4%)	1.19 (16%)	1.47 (20%)
42040	U_5 (m/s)	-1.97 (-15%)	1.98 (15%)	2.14 (17%)
	H_s (m)	-0.90 (-18%)	0.90 (18%)	1.01 (21%)
	T_m (s)	-0.26 (-3%)	0.50 (7%)	0.58 (8%)
Sandy (2012): 41001	U_5 (m/s)	n/a	n/a	n/a
	H_s (m)	0.76 (10%)	1.13 (15%)	1.42 (18%)
	T_m (s)	-0.11 (-1%)	0.44 (5%)	0.53 (6%)
41002	U_5 (m/s)	0.96 (6%)	1.65 (10%)	2.00 (12%)
	H_s (m)	0.09 (1%)	0.61 (10%)	0.72 (11%)
	T_m (s)	-0.36 (-4%)	0.49 (6%)	0.59 (7%)
41010	U_5 (m/s)	0.45 (4%)	1.02 (8%)	1.27 (10%)
	H_s (m)	-0.05 (-1%)	0.52 (10%)	0.70 (14%)
	T_m (s)	-0.05 (-1%)	0.61 (8%)	0.70 (9%)
41047	U_5 (m/s)	-0.56 (-4%)	1.21 (8%)	1.46 (10%)
	H_s (m)	0.35 (6%)	0.50 (8%)	0.70 (12%)
	T_m (s)	0.05 (1%)	0.43 (5%)	0.52 (6%)
41048	U_5 (m/s)	1.77 (11%)	2.11 (13%)	2.53 (16%)
	H_s (m)	0.04 (0%)	0.58 (8%)	0.76 (10%)
	T_m (s)	-0.25 (-3%)	0.42 (5%)	0.55 (6%)
44009	U_5 (m/s)	1.95 (11%)	2.18 (13%)	2.85 (17%)
	H_s (m)	-0.18 (-4%)	0.67 (13%)	0.78 (16%)
	T_m (s)	-0.40 (-6%)	0.59 (8%)	0.74 (11%)
44025	U_5 (m/s)	0.96 (6%)	2.18 (13%)	3.07 (18%)
	H_s (m)	0.05 (1%)	1.15 (22%)	1.34 (25%)
	T_m (s)	-0.49 (-6%)	0.99 (13%)	1.09 (14%)

timing and general features of the eye and eyewall of Ike quite well as shown by the wind speed and direction at both locations (Figs. 2a, b and 3a, b). The model wind speed was weaker early on 10 and 11 September prior to the arrival of Ike at 42001, indicating that the size of the hurricane may be smaller in the model than that of observations (Fig. 2a), which is consistent with the under-prediction of significant wave height and mean period (Fig. 2c and d). The peak winds associated with the eyewall in the model were slightly higher than the observation, and so were the significant wave height and mean period at 42001 from 1600 UTC 11 September to 0600 UTC 12 September. However, the modeled significant wave height is about 3–4 m higher than the observed value during the passage of the hurricane eyewall at 2000 UTC on 11 September and 0300 UTC on 12 September (Fig. 2c), which is more than what can be accounted for the difference in wind speed (Fig. 2a). Another factor contributing to the overestimate of wave height may be faster storm translation speed in the model (Fig. 1a), which can increase the effective fetch. A faster moving storm is in resonance with longer waves, which can then grow longer and higher for the same wind speeds. There is an indication of a similar situation at 42035, although the

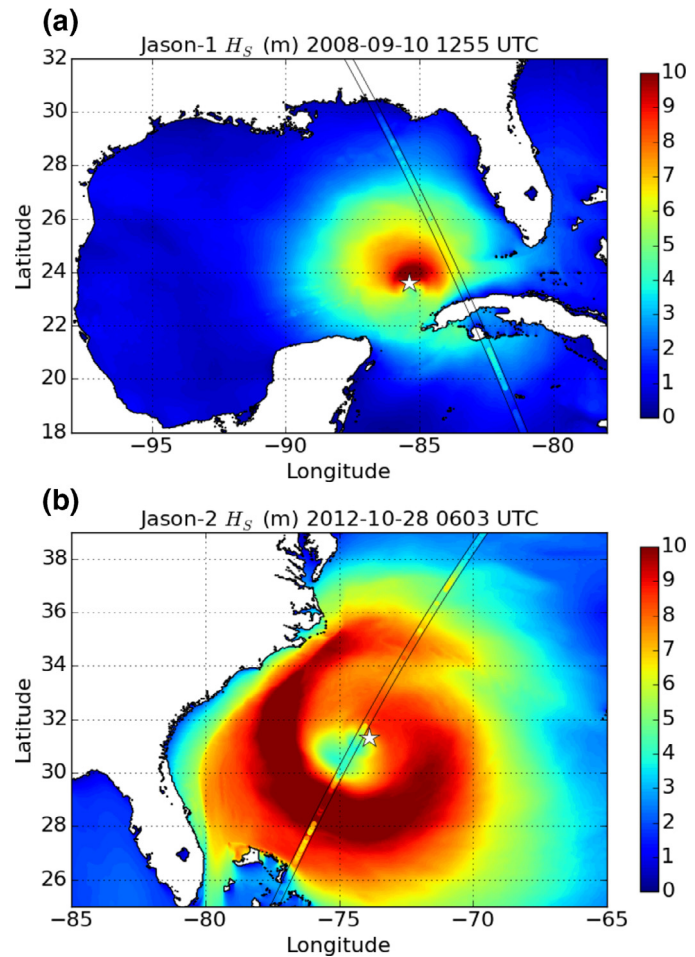


Fig. 6. Significant wave height (H_s , m, shown in color) from UWIN-CM: (a) Hurricane Ike at 0500 UTC on 10 September 2008 and (b) Superstorm Sandy at 0600 UTC on 28 October 2012. The H_s observations from Jason-1 and Jason-2 satellite overpasses (marked by the two thin black lines) are overlaid on the model prediction. The star symbol marks the UWIN-CM predicted center of each storm.

buoy did not report the wave data during the peak of the storm near landfall (Fig. 3c).

The NDBC buoys 41002 and 41048 were located on the left and right side of the storm track during Sandy on 27–30 October 2012 (Fig. 1b). The modeled wind speed and wave height and period at these two locations were very close to the observed values (Figs. 4 and 5). Sandy was an unusually large storm with tropical storm winds over a vast region of the West Atlantic basin (Blake et al., 2013). While the modeled wind speed was of similar magnitude at buoys 41002 and 41048, the significant wave height was 1–2 m higher than the observations, perhaps due to longer fetch in the observed storm.

The overall performance of the model at all 14 buoy locations is summarized in Table 1. We compute model bias, mean absolute error, and root mean squared error for the wind, significant wave height, mean wave period, averaged over the model simulation/prediction time periods (~5 days in Ike and 2.5 days in Sandy). Overall, UWIN-CM performed better in Sandy (41001–44025) compared to Ike (42001–42040). There is a small positive bias in significant wave height (2% on average), and a small negative bias in mean period (−2% on average).

Spatial variation of the significant wave height in hurricanes can be derived from the satellite radar altimetry data that measures

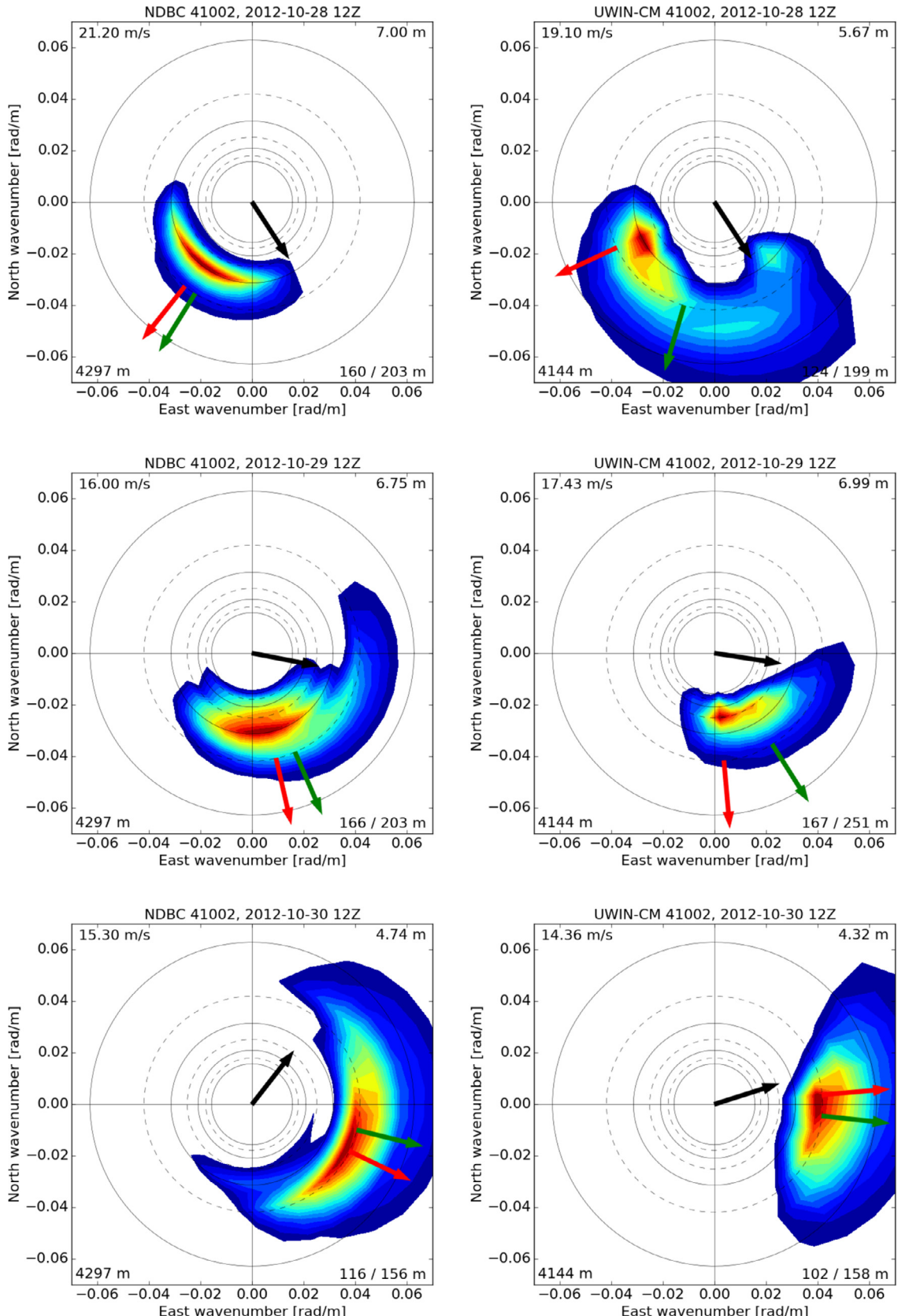


Fig. 7. Comparisons of observed (left panels) and UWIN-CM predicted (right panels) directional wave spectrum at NDBC buoy 41002 in Superstorm Sandy at 1200 UTC 28 October 2012 (top panels), 1200 UTC 29 October 2012 (middle panels), and 1200 UTC 30 October 2012 (bottom panels). The color shading starts at 10% of the peak (blue), increasing linearly at 10% increments until the peak value (red). The circles indicate wavelengths at 50 m interval, starting from 100 m from the outermost circle and ending at 400 m with the innermost circle. The black arrow indicates wind direction, while the green and red arrows indicate mean and peak wave direction, respectively. The values in the corners indicate local wind speed (upper left), significant wave height (upper right), mean and peak wavelength (lower right) and mean water depth (bottom right). (For interpretation of the references to colour in this figure legend, the reader is referred to the web version of this article.)

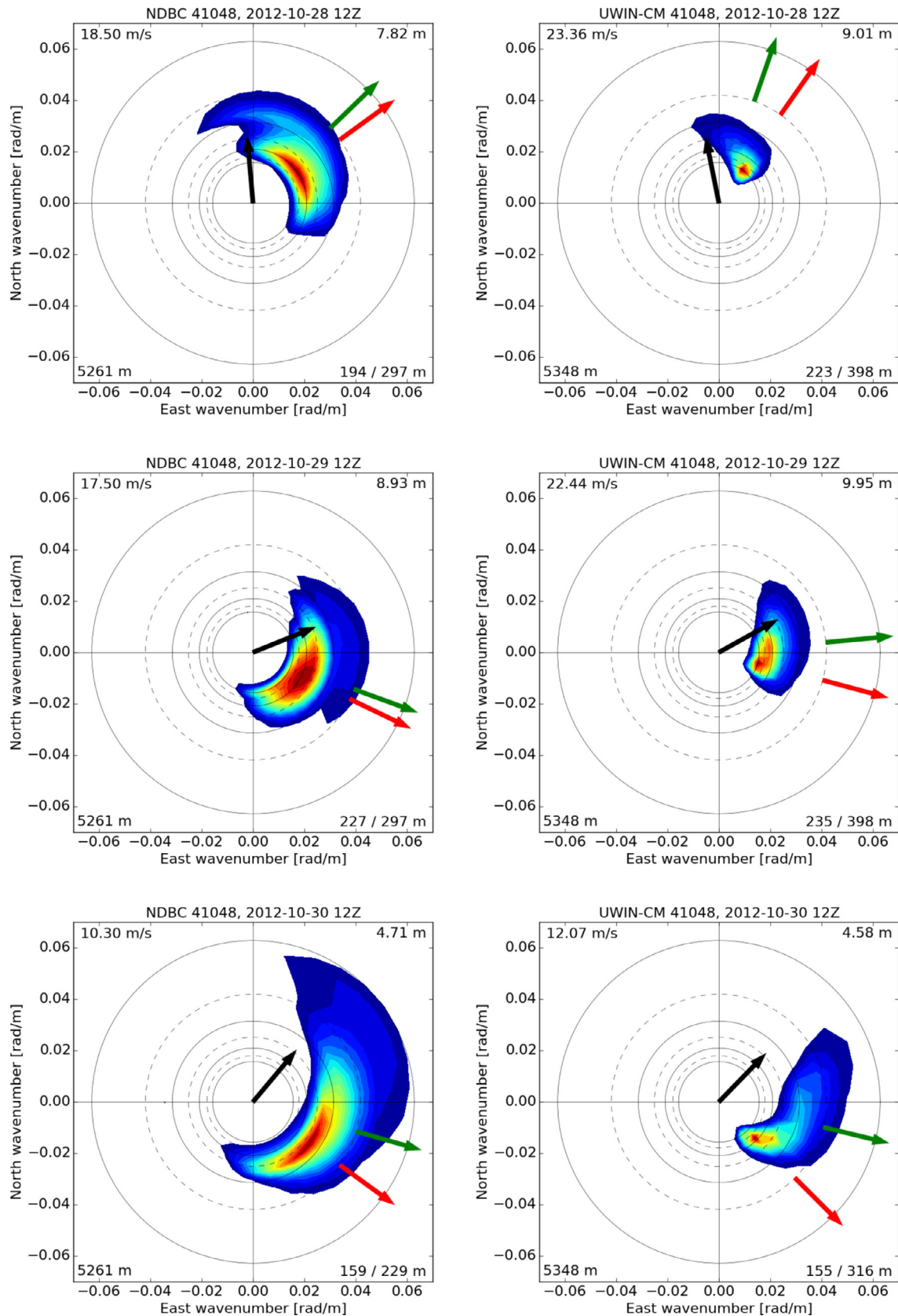


Fig. 8. Same as in Fig. 7, except for NDBC buoy 41048. (For interpretation of the references to colour in this figure legend, the reader is referred to the web version of this article.)

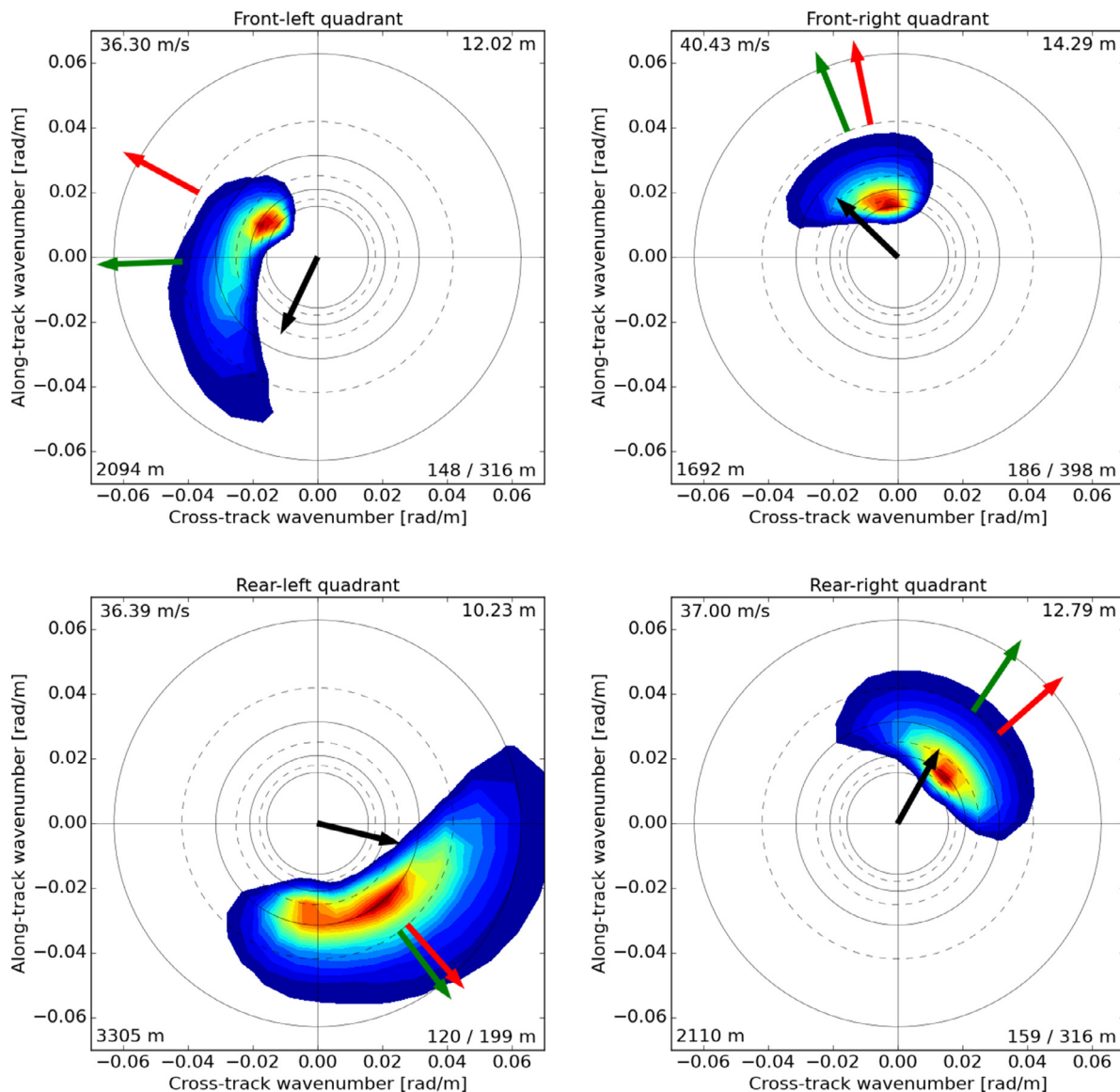


Fig. 9. UWIN-CM simulated directional wave spectrum in four quadrants in Hurricane Ike, 70 km from the center, at 1200 UTC 11 September 2008 when Ike was located over the open ocean. The elements on each panel have the same meaning as of those in Figs. 7 and 8. The spectrum and wind direction are rotated relative to storm motion so that the up direction corresponds to the front of the storm. (For interpretation of the references to colour in this text, the reader is referred to the web version of this article.)

the ocean surface topography. Overpasses of Jason-1 and Jason-2 were available in Hurricane Ike at 1255 UTC on 10 September 2008, and in Superstorm Sandy at 0603 UTC on 28 October 2012, respectively. The satellite data have a spatial resolution of 11.2 km (along track) and 5.1 km (cross track). We use the altimeter data to compare with the UWIN-CM simulated H_s in Ike and Sandy (Fig. 6). To evaluate hurricane-induced wave field, we compare the modeled H_s at the same geographical location as the satellite observation. The model predicted track in Ike was several hours faster than the best track estimate (Fig. 1a). So the comparison uses the UWIN-CM field at 0500 UTC on 10 September when the modeled storm was at the same location as the observation (Fig. 6a). The UWIN-CM predicted storm track in Sandy is accurate and the model and observation are compared at the same time and location (Fig. 6b). The model prediction of spatial pattern of H_s in both Ike and Sandy were in excellent agreement with the satellite observations. The H_s pattern in Ike was typical of a moving hurricane with high waves in the right-front quadrant (Fig. 6a) as shown in previous studies

(Stopa et al., 2012; Chen et al., 2013). The highest H_s values were predicted to be at the two rear quadrants where the strongest winds were located in Sandy, which was confirmed by the altimeter data (Fig. 6b).

5. Spatial variation of directional wave spectrum in open ocean

To contrast the characteristics of hurricane-induced ocean surface waves in open ocean to that at landfall, we first investigate the directional wave spectrum on different sides of the storm track in Sandy. These pitch-and-roll buoys have a 3-m discus hull and record time series of surface elevation as well as the surface slope in two directions (Steele et al., 1992). We use the Longuet-Higgins (1963) Fourier expansion method (FEM) coefficients provided by NDBC to reconstruct the directional wave spectrum. The coupled model results are compared with the directional wave spectrum measurements obtained at the 41002 and 41048 buoys from three different times during the storm's passage (Figs. 7 and 8). The wind

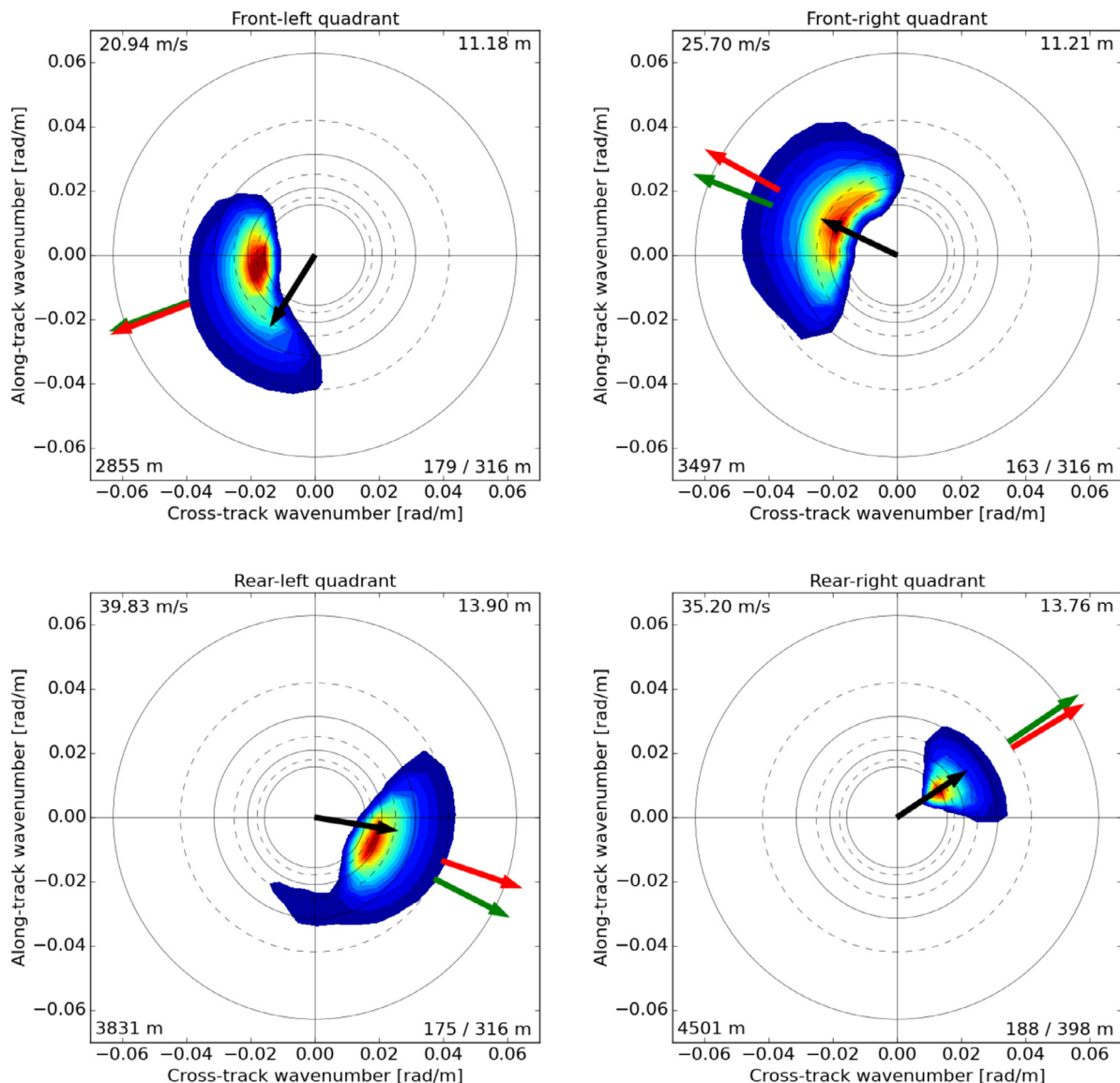


Fig. 10. Same as in Fig. 9, except for Superstorm Sandy at 1800 UTC 29 October 2012 when Sandy was over the open ocean. Each panel corresponds to a location 150 km from the storm center, in its respective quadrant. (For interpretation of the references to colour in this text, the reader is referred to the web version of this article.)

direction changed gradually counter-clockwise at 41002 and clockwise at 41048 as Sandy moved through the area, followed by slower turning of the wave field. Overall, UWIN-CM produced the observed directional wave spectrum in terms of wavelength and mean and dominant wave directions. The observed spectrum is generally wider in the directional space, which is partially an artifact of the limited sampling capabilities of a pitch-and-roll buoy (Young, 1994). There is a large misalignment between wind (black arrow) and both mean (green arrow) and peak (red arrow) wave direction at both locations, likely due to the large spatial coverage of Sandy's wind field.

Spatial distribution of directional wave spectrum in hurricanes is especially important in coupled atmosphere-wave-ocean models like UWIN-CM, because the wave field affects the wind through wind-wave stress in coupled models (Chen et al., 2013). Here we examine the spatial variations of the wave spectrum around the center of the storm in both Ike (Fig. 9) and Sandy (Fig. 10). The wave spectrum is shown in each of the four quadrants around the storm relative to the storm heading direction: front-right (FR), front-left

(FL), rear-right (RR), and rear-left (RL). In the example of Ike at 0000 UTC on 12 September, the wave spectrum is shown at 70 km radius from the storm center in each quadrant (Fig. 9). The waves are longest and highest in the FR quadrant, and shortest and lowest in the RL quadrant. Significant wave height in the FR quadrant is 15% higher than that in FL and RR, and 40% higher than that of RL. The wind speed is 10% higher in the FR quadrant relative to other three quadrants, which is a common feature in hurricanes due to the storm motion (e.g., Shapiro, 1983; Chen et al., 2006). The directions of the dominant waves are outward (red arrow) between 20° and 30° clockwise from local wind direction (black arrow). The spectrum is broadest in the RL, where the longer waves are in the opposite direction to the local wind, spanning nearly 180° in directional space while the wavelengths range from under 100 to over 350 m. The mean wave direction (green arrow) was between dominant wave and wind directions. The characteristics of directional wave spectrum described here are in agreement with those observed in Hurricane Bonnie (1998) in the open ocean by Wright et al. (2001).

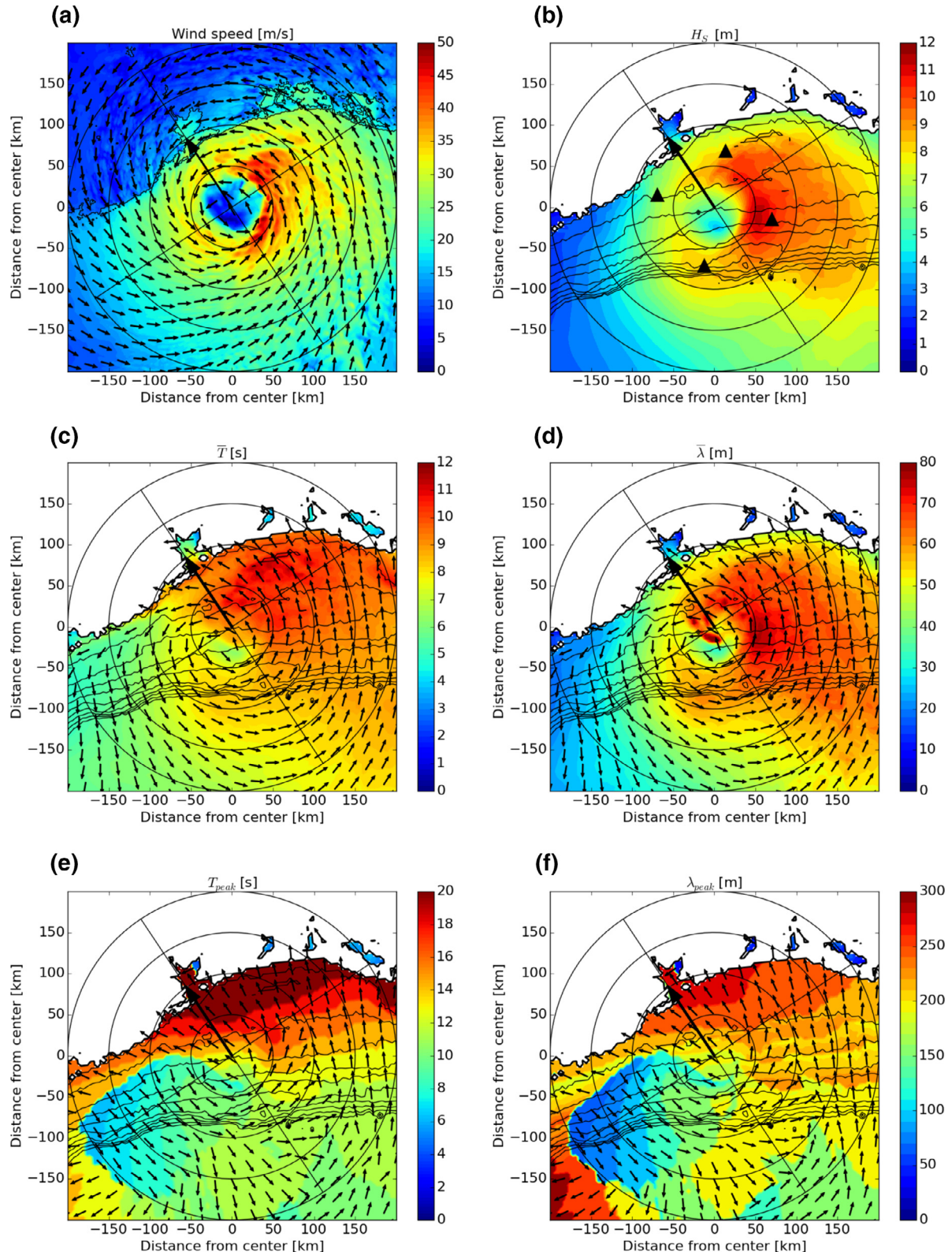


Fig. 11. UWIN-CM simulated (a) 10-m wind speed, (b) significant wave height, (c) mean wave period, (d) mean wavelength, (e) peak wave period, and (f) peak wavelength in Hurricane Ike at 1800 UTC 12 September 2008. The black vectors represent wind direction in (a), mean wave direction in (c, d) and peak wave direction in (e, f). Thin black lines are isobaths between 10 m and 100 m at 10 m intervals, with lower values near the coast and higher values offshore. The large black arrow indicates the direction of storm heading. The black triangles in panel (b) indicate the locations of directional spectrum analysis shown in Fig. 14.

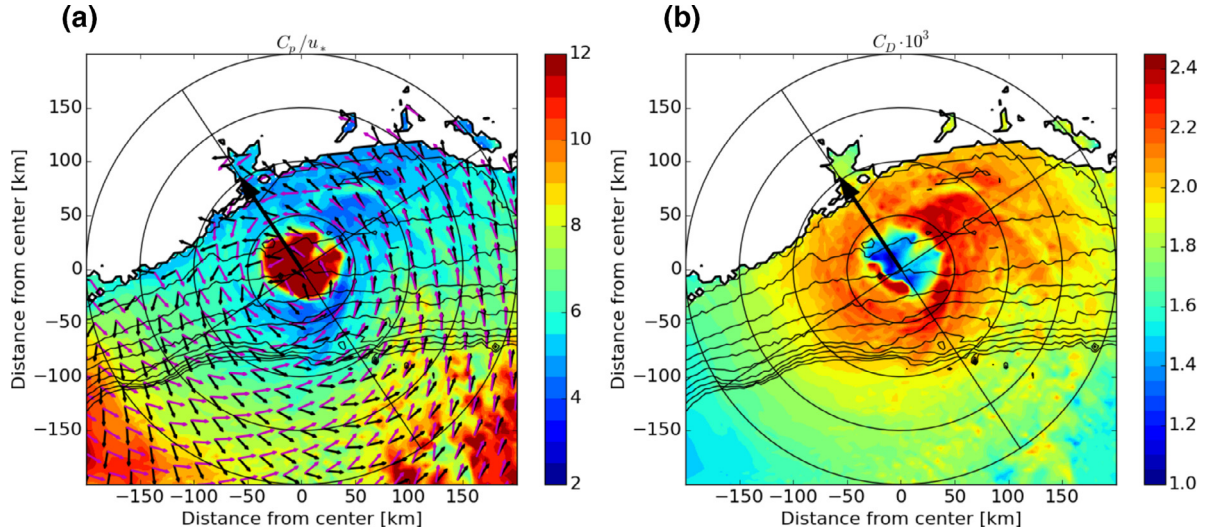


Fig. 12. UWIN-CM simulated (a) wave age and (b) drag coefficient in Hurricane Ike near landfall at 1800 UTC on 12 September 2008.

The directional wave spectrum in the open ocean during Sandy is very different from that in Ike as shown in the example from UWIN-CM forecast at 1800 UTC on 29 October 2012 (Fig. 10). The storm was heading toward north–northwest, while the strongest wind was located in the southern side (RL and RR quadrants) due to its interaction with the extratropical system. The highest H_s values were located in the two rear quadrants (Fig. 6b). Spectra in all quadrants are narrower than those in Ike (Fig. 9), and are rotated by about 30° counter-clockwise, with the exception of RR, where the waves were propagating in the similar direction as in Ike. The RR quadrant is also where the waves are the longest, with very narrow directional spreading. The narrow wave spectrum may be explained by a wide swath of strong wind blowing from RL to RR as observed by the OSCAT satellite wind (Blake et al., 2013).

6. Wave properties near landfall

Hurricane impacts are mostly felt at landfall, which are also most challenging for accurate model forecasts of extreme winds, rain, waves, storm surge, and inland flooding near the coast. Ocean surface waves play an important role in storm surge (Luettich, 1999; Hsu, 2013), especially in the cases of Ike (2008) and Sandy (2012) when the water levels were elevated by the wave set up and the large size of the storm winds, which were not represented by the uncoupled models as pointed out by Alves et al. (2015). Wave set-up has been found to contribute to total storm surge from 15% in Hurricane Floyd (1999) (Funakoshi et al., 2008) to 40% in Typhoon Anita (2010) (Kim et al., 2010). UWIN-CM has the advantage of the atmosphere–wave–ocean coupling that can potentially produce the coherent wind–wave and wave–current interactions needed for hurricane impact forecasting at landfall. As storms approach the land, the wind and wave fields become more complex, in part due to the coastal land–sea features including topography and bathymetry. Here we focus on the spatial distribution of ocean surface waves and corresponding wind and water depth near landfall in Ike and Sandy.

6.1. Hurricane Ike

At 1800 UTC on 12 September, Ike was approaching the Texas coast, the UWIN-CM modeled 10-m wind field was asymmetric, with highest wind speeds exceeding 45 m/s on the right-hand side of the

storm (Fig. 11a). Significant wave height was significantly higher on the right side with the maximum exceeding 11 m in the RR quadrant right outside of the radius of maximum wind (Fig. 11b). The wave heights were reduced in front of the storm as they approach the coast, where they dissipate due to breaking, and to a lesser extent, bottom friction. The mean periods of the longest waves exceeding 10 s are located in the FR quadrant (Fig. 11c), as was observed in Hurricane Bonnie by Walsh (2002) and Wright et al. (2001). As waves enter shallower waters, they decrease in wavelength while preserving the periods due to conservation of wave crests (Fig. 11d). The waves were significantly shorter on the left side of the storm center due to very short fetch from the offshore wind. The peak period and wavelength (Fig. 11e and f) showed strong asymmetry between the left and right sides of the storm, with waves exceeding 250 m in wavelength on the right side, while being constrained between 50 and 100 m wavelength on the left. The depth decreases from 100 m to the sea level over a distance of approximately 150 km on the left and 200 km on the right side of the storm, respectively.

Despite the large wind speed asymmetry, wave age C_p/u_* and drag coefficient C_D are fairly symmetric, suggesting that the wave-state is young and rough on the left in the shallow water near the coast (Fig. 12). Because friction velocity u_* scales with wind speed squared, wave age has its lowest values where the wind forcing is strongest. The second contributing factor in reducing wave age is the water depth. Both the decrease in wave age and the increase in C_D come from a phase speed reduction in shallow water. The enhancement of C_D on the left was due, in part, to the offshore wind forcing over limited fetch, as young windsea carries more stress than the long swell (Donelan et al. 2012). Another mechanism that may be responsible for the increase of the drag coefficient is the opposing and cross-wind swell, as found in the FL quadrant (Fig. 11e). Wind blowing against incoming swell induces upward flux of horizontal momentum, i.e. momentum transfer from waves to wind, effectively damping wave energy and increasing stress. A strong increase in C_D in the FL quadrant where opposing and cross-wind swell dominates was reported by Holthuisen et al. (2012). We find that the drag coefficient in shallow water (depth <20 m) may be increased from 4% in high wind speed, up to 25% in low wind speeds, relative to that of deep water (Fig. 13a). This is in agreement with in situ measurements by Zachry et al. (2013) who found high values of C_D during landfall of Ike. Similar pattern in C_D as function of wind speed can be found by contrasting wave properties from the left and right

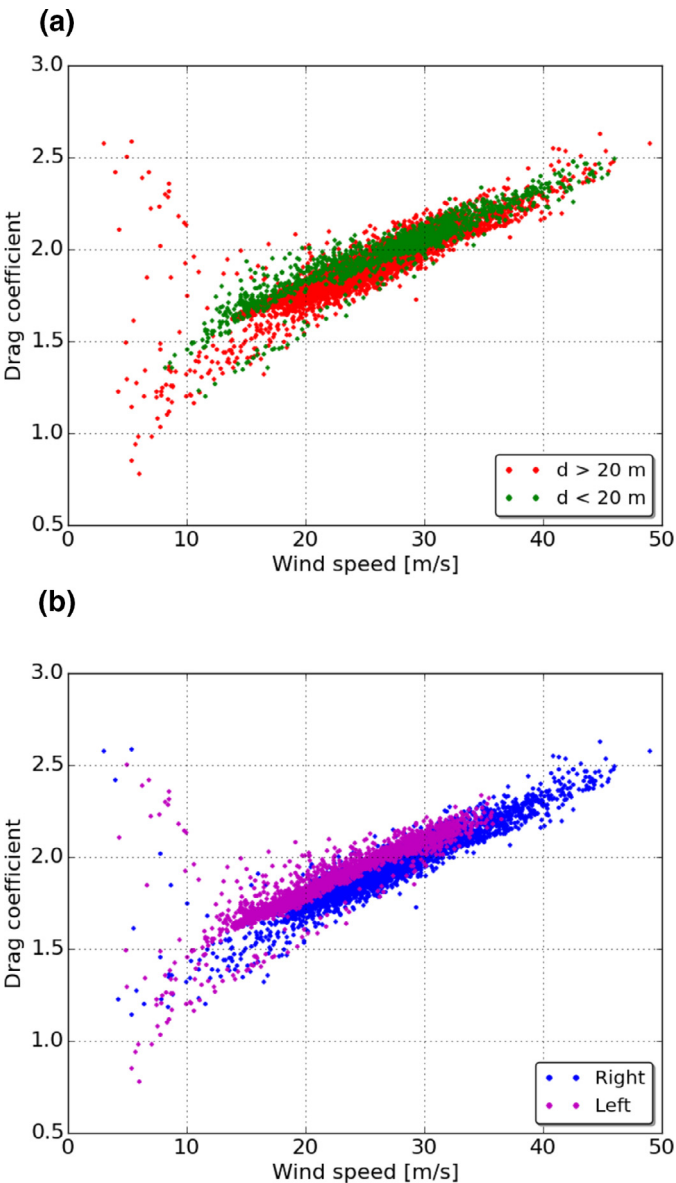


Fig. 13. UWIN-CM simulated drag coefficient as function of 10-m wind speed in Hurricane Ike valid at the same time as in Fig. 11, stratified by (a) water of depth greater than 20 m (red) and less than 20 m (green), and (b) locations on the left (magenta) and right (blue) side of the storm. (For interpretation of the references to colour in this figure legend, the reader is referred to the web version of this article.)

side of the storm (Fig. 13b). Thus, as the storm approaches landfall, stress is likely to increase in the front quadrants due to water depth decrease, and increase even further in the FL quadrant where offshore wind forces young windsea and opposes long incoming swell.

As Hurricane Ike enters shallow water, several interesting properties in the directional wave spectrum arise (Fig. 14). The peak waves in the front quadrants rotate clockwise toward the coast, subject to depth-induced refraction, increasing the misalignment with wind by as much as 30° in the FL quadrant. The spectrum becomes broader in all four quadrants compared to that in deep water, and the peak waves are even more misaligned with the wind. While the peak wavelength in the rear quadrants is similar to that in deep water, it is significantly reduced in the front quadrants where waves shoal and dissipate as they propagate into shallow water. Because the

depth-induced wave breaking and bottom friction are prominent in front of the storm, the highest significant wave height is found in the RR quadrant, and is 27% higher relative to that of RL and FR quadrants, and 65% higher than that of FL quadrant. Besides wave breaking and bottom friction, the waves in the FL quadrant were also dissipated by the opposing wind. Finally, the spectrum is least affected by the water depth in the RL quadrant.

The UWIN-CM predicted wave fields compare well with the wave and surge hindcast results in Hope et al. (2013) in general, with a few notable differences. First, the UWIN-CM predicted wind field near Ike's landfall is more asymmetric than the H*WIND analysis field used in Hope et al., while the peak wind speeds are comparable. The difference in the wind fields may have contributed to a more asymmetric wave height in UWIN-CM, with lower H_s on the left side of the storm track (Fig. 11b). It is difficult to make a meaningful comparison between the coupled model prediction of interactive wind and waves with the hindcast wave fields using a non-interactive wind analysis product. Donelan et al. (2012) found that H*WIND overestimated high wind speeds in multiple locations in Hurricane Ike.

6.2. Superstorm Sandy

As Sandy approached the northeast coast of the United States as a Category 1 hurricane, its wind field was unusually broad and asymmetric (Fig. 15a). The strong wind dominates the FL, RL, and RR quadrants, exceeding 35 m/s. As a consequence, the significant wave height was very large, with highest waves exceeding 12 m in the RR quadrant (Fig. 15b). The local minimum in the wake of the storm center was not as clearly defined as in Ike. The wave heights decreased toward shallower water, and were smaller near coast by approximately factor of 2 compared to the peak wave heights on the right side of the storm, which is consistent with observations by Walsh et al. (2002). The longest waves were spread out across the front and right sides of the storm and were streamed along the Hudson Canyon toward the New York Bight (Fig. 15f).

The directional wave spectrum in the front quadrants showed that the waves dissipate, contract, and refract toward the coast as they propagate over the continental shelf (Fig. 16). The wave spectrum in the front quadrants was rotated clockwise toward the coast in a similar manner as we found in Ike (Fig. 13). The spectra in RR are now bi-modal and significantly broader than 8 h earlier, possibly because of the increase in misalignment between mean and dominant wave directions. The RL quadrant is the least changed, likely because of strong and persistent wind forcing that dominated in this region (Fig. 15a).

7. Summary and conclusions

The high-resolution, fully coupled atmosphere-wave-ocean model UWIN-CM was used to simulate and predict the hurricane-induced ocean surface waves in Hurricane Ike (2008) and Superstorm Sandy (2012) at landfall 3–5 days in advance. The model output is used to better understand the spatial distribution of the integrated mean wave properties (significant wave height and mean wave period) and the directional wave spectra over the open ocean and near landfall. The unusual spatial pattern of significant wave height in Sandy was well predicted by the coupled model as confirmed by Jason-2 satellite altimeter data (Fig. 6b). The coupled model prediction is also evaluated using NDBC buoy measurements during the time of the storm passages. While both storms were well represented by UWIN-CM in terms of the wind and waves, the model performance was slightly better in the case of Sandy. Overall, the average root mean squared error for the wind speed, significant wave height, and wave period were $2.24 (\pm 0.81)$ m/s, $0.98 (\pm 0.36)$ m, and $1.01 (\pm 0.45)$ s, respectively (Table 1).

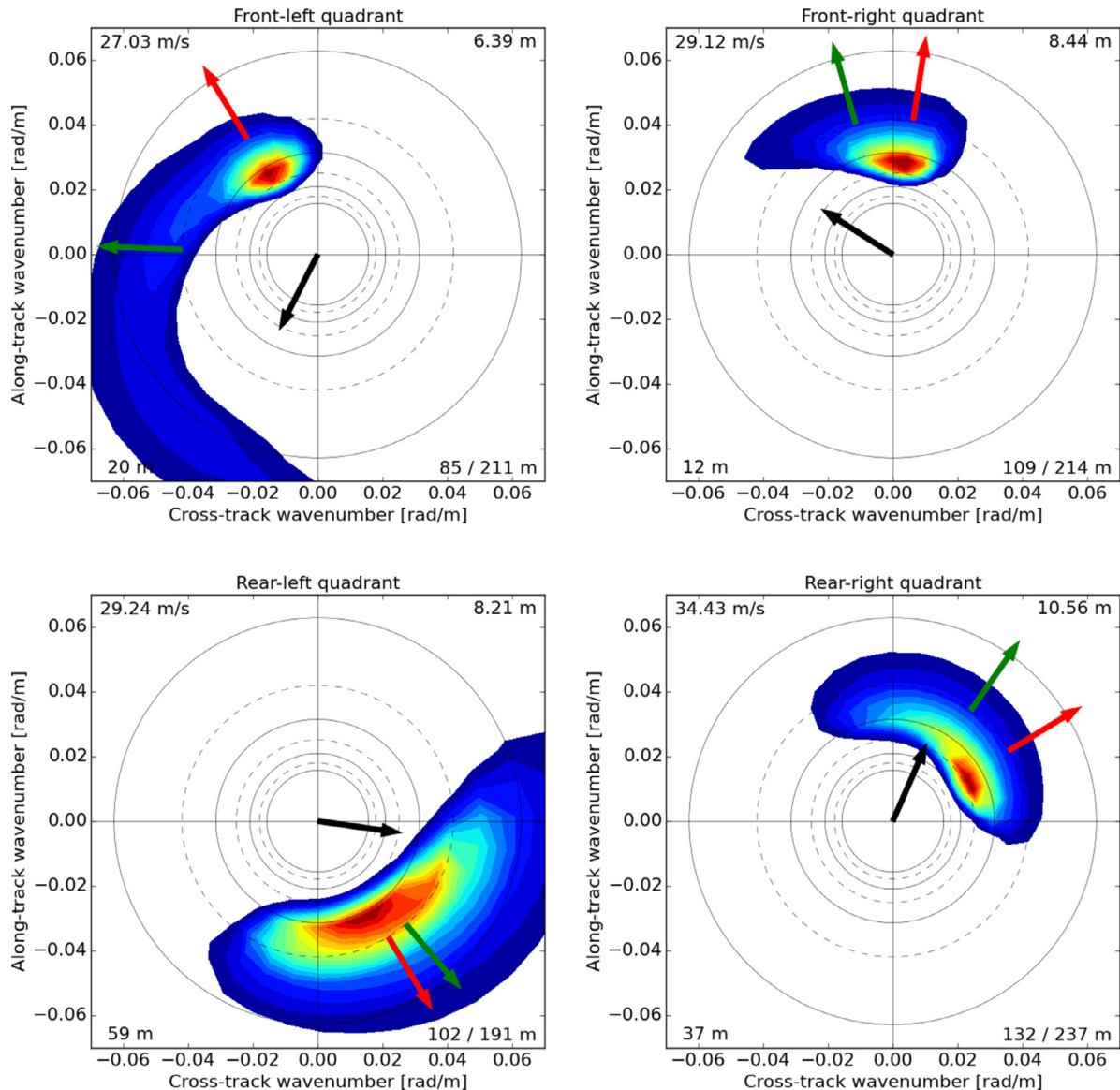


Fig. 14. Same as in Fig. 9, except for 1800 UTC 12 September 2008 when Hurricane Ike was approaching the Texas coast.

We find that as the hurricane-induced waves propagate into progressively shallower water, they shoal, dissipate, and refract, resulting in an overall broader and more complex directional spectrum compared to that of the open ocean. Shoaling and dissipation can decrease the wavelength and energy of all waves in front of the storms as they propagate into shallow water. Depth-induced refraction turns the waves toward the direction perpendicular to the iso-baths. While the decrease in wave celerity due to change in water depth leads to an increase in wind stress, refraction turns the dominant waves away from wind and toward the coast, thus increasing misalignment between wind and waves on the left side of the storm center. This increase in misalignment is the largest in the front-left quadrant where the winds are generally blowing off shore. It is as large as 30° in Ike and 60° in Sandy. Waves propagating against wind induce upward momentum flux, further increasing stress while getting damped. These two processes are found to contribute together to an increase in drag coefficient by up to 25%, especially on the left side of the storm center in Hurricane Ike at landfall (Fig. 13).

The directional wave spectrum in the four quadrants around Ike in deep water is found to be consistent with the established model of hurricane-induced ocean waves (Wright et al., 2001; Chen et al., 2013). However, as the storm approaches landfall, spectra in all quadrants become broader and more complex, and the misalignment between wind and waves increases. The waves in Sandy were significantly more symmetric in terms of wave height and wavelength compared with those in Ike, mainly because of the strong asymmetric wind in the South region of the storm compensating the typical asymmetry in the wave field. While Walsh et al. (2002) found the spectra in open ocean and near landfall to be similar in Hurricane Bonnie (1998), and suggested that parameterization of the wave fields in prediction models with simple storm parameters may be satisfactory, the results shown in this study suggest that the waves near landfall becomes more complex than in the open ocean because of the changes in water depth and wind fields that are storm and location dependent. These pose many challenging issues for modeling and predicting the fully coupled wind and wave phenomena in hurricanes near landfall.

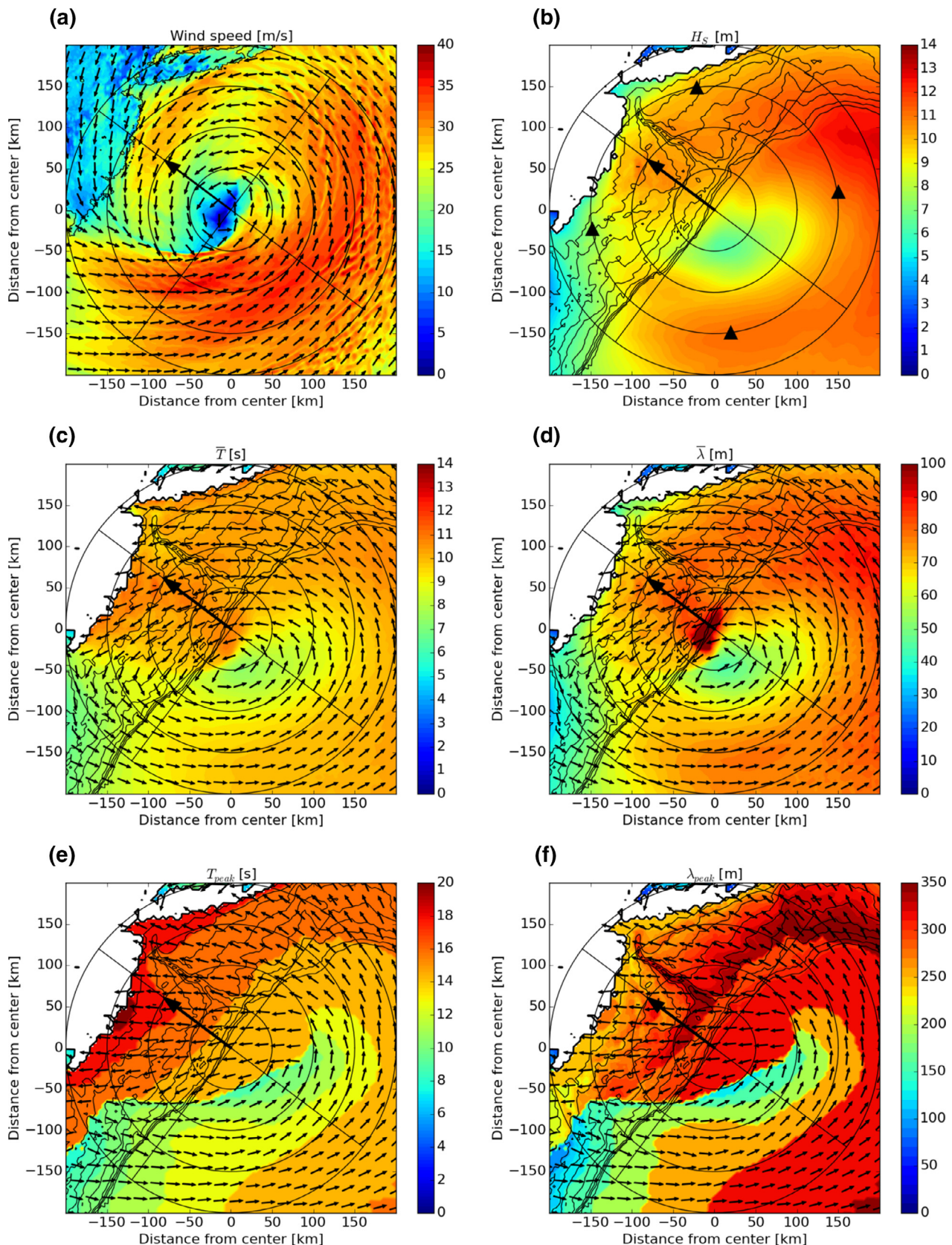


Fig. 15. Same as in Fig. 11, except for Superstorm Sandy at 0200 UTC on 30 October 2012. The black triangles in panel (b) indicate the locations of directional spectrum analysis shown in Fig. 16.

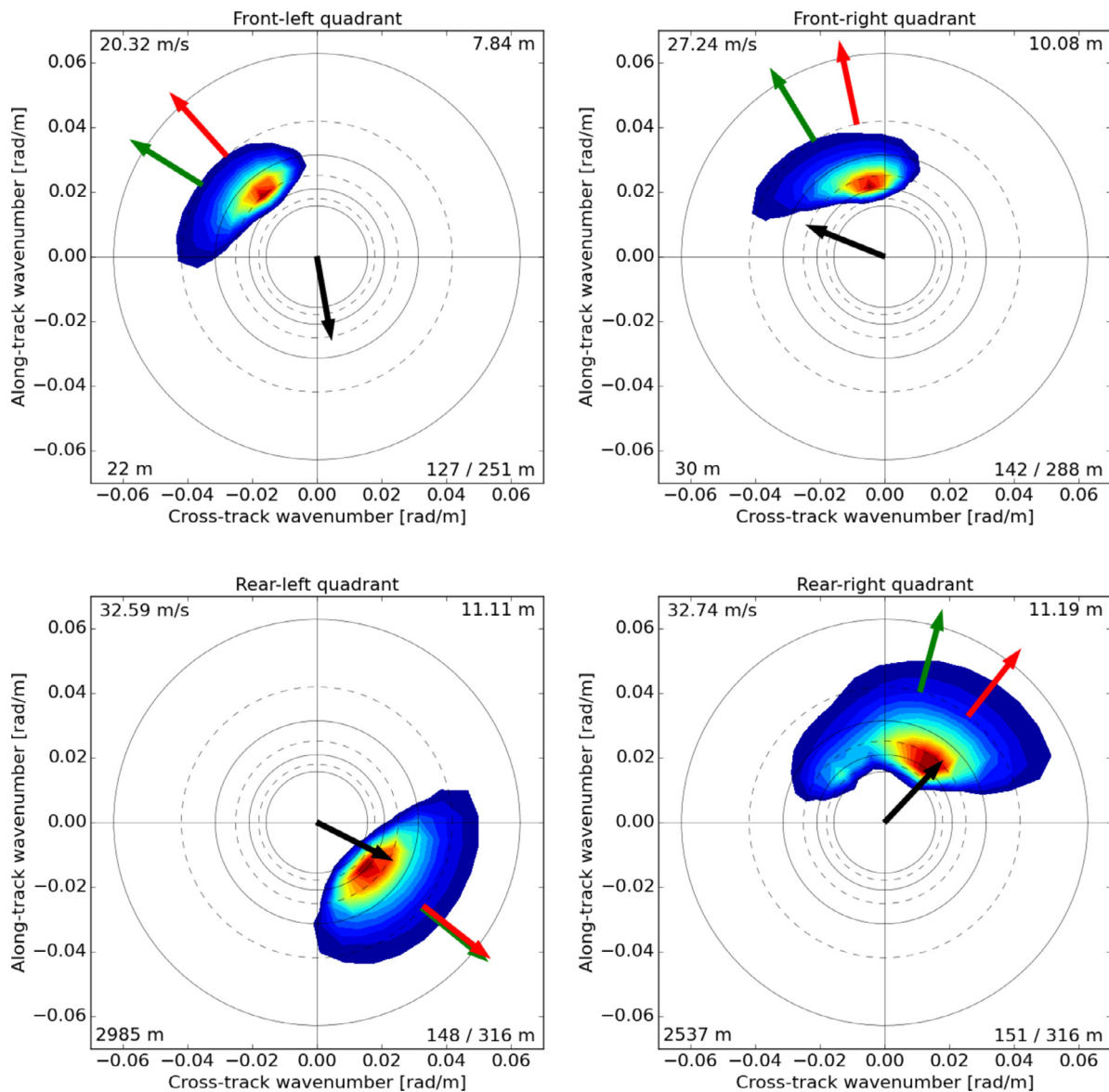


Fig. 16. Same as in Fig. 10, except for Superstorm Sandy near landfall at 0200 UTC on 30 October 2012.

Acknowledgments

We thank Mark Donelan for his contribution to the development of the University of Miami Wave Model, Tim Campbell for his input on the design of the Unified Wind INterface (UWIN) in the coupled model UWIN-CM, and John Michalakes for his input on the WRF model during the early stage of this study. Comments and suggestions from three anonymous reviewers have helped improve the manuscript. This research was supported by research grants from the [Office of Naval Research](#) under the National Oceanography Partner Program (NOPP N0001401010162), the National Renewable Energy Lab/[Department of Energy](#) (DOE FOA 415), NASA Ocean Vector Wind Science Team (NNX14AM78G), and a grant from [BP/The Gulf of Mexico Research Initiative](#).

References

- Alves, J.-H.G.M., Stripling, S., Chawla, A., Tolman, H., van der Westhuysen, A., 2015. Operational wave guidance at the US National Weather Service during tropical/post-tropical storm Sandy, October 2012. *Mon. Weather Rev.* 143, 1687–1702.
- Blake, E.S., Kimberlain, T.B., Berg, R.J., Cangialosi, J.P., Beven, J.L., 2013. Tropical Cyclone Report: Hurricane Sandy (AL182012). National Hurricane Center Technical Report.
- Chen, S.S., Knaff, J., Marks, F.D., 2006. Effect of vertical wind shear and storm motion on tropical cyclone rainfall asymmetry deduced from TRMM. *Mon. Weather Rev.* 134, 3190–3208.
- Chen, S.S., Price, J.F., Zhao, W., Donelan, M.A., Walsh, E.J., 2007. The CBLAST-Hurricane program and the next-generation fully coupled atmosphere–wave–ocean models for hurricane research and prediction. *Bull. Am. Meteorol. Soc.* 88, 311–317.
- Chen, S.S., Zhao, W., Donelan, M.A., Tolman, H.L., 2013. Directional wind-wave coupling in fully coupled atmosphere–wave–ocean models: results from CBLAST-hurricane. *J. Atmos. Sci.* 70, 3198–3215.
- Donelan, M.A., Curcic, M., Chen, S.S., Magnusson, A.K., 2012. Modeling waves and wind stress. *J. Geophys. Res.* 117, C00J23. doi:10.1029/2011JC007787.
- Earle, M.D., January 1996. Nondirectional and Directional Wave Data Analysis Procedures. Stennis Space Center, MS NDBC Technical Document 96-01.
- Funakoshi, Y., Hagen, S.C., Bacopoulos, P., 2008. Coupling of hydrodynamic and wave models: case study for Hurricane Floyd (1999) hindcast. *J. Waterw. Port Coast. Ocean Eng.* 134 (6), 321–335.
- Hill, C., DeLuca, C., Balaji, V., Suarez, M., da Silva, A., 2004. The architecture of the Earth system modeling framework. *Comput. Sci. Eng.* 6, 18–28.
- Holthuijsen, L.H., Powell, M.D., Pietrzak, J.D., 2012. Wind and waves in extreme hurricanes. *J. Geophys. Res.* 117, C00J23. doi:10.1029/2012JC007983.
- Hong, S.-Y., Dudhia, J., Chen, S.-H., 2004. A revised approach to ice microphysical processes for the bulk parameterization of clouds and precipitation. *Mon. Weather Rev.* 132, 103–120.

- Hong, S.-Y., Noh, Y., Dudhia, J., 2006. A new vertical diffusion package with an explicit treatment of entrainment processes. *Mon. Weather Rev.* 121, 2318–2341.
- Hope, M.E., et al., 2013. Hindcast and validation of Hurricane Ike (2008) waves, forerunner, and storm surge. *J. Geophys. Res. Oceans* 118, 4424–4460. doi:10.1002/jgrc.20314.
- Hsu, S., 2013. Storm surges in New York during hurricane Sandy in 2012: a verification of the wind-stress tide relation. *Boundary Layer Meteorol.* 148 (3), 593–598.
- Kain, J.S., Fritsch, J.M., 1993. Convective parameterization for mesoscale models: the Kain–Fritsch scheme. In: Emanuel, K.A., Raymond, A.M.S.D.J. (Eds.), *The Representation of Cumulus Convection in Numerical Models*, p. 246.
- Kim, S.Y., Yasuda, T., Mase, H., 2010. Wave set-up in the storm surge along open coasts during Typhoon Anita. *Coastal Eng.* 57, 631–642.
- Large, W.G., McWilliams, J.C., Doney, S.C., 1994. Oceanic vertical mixing: a review and a model with a nonlocal boundary layer parameterization. *Rev. Geophys.* 32, 363–403.
- Longuet-Higgins, M.S., Cartwright, D.E., Smith, N.D., 1963. Observations of the directional spectrum of sea waves using the motions of a floating buoy. *Ocean Wave Spectra*. Prentice-Hall, Englewood Cliffs, NJ.
- Luettich Jr., R.A., Westerink, J.J., May 1999. Implementation of the Wave Radiation Stress Gradient as a Forcing for the ADCIRC Hydrodynamic Model: Upgrades and Documentation for ADCIRC Version 34.12. Department of the Army, US Army Corps of Engineers, Waterways Experiment Station, Vicksburg, MS, p. 9 Contractors Report.
- Powell, M.D., Houston, S.H., Amat, L.R., Morisseau-Leroy, N., 1998. The HRD real-time hurricane wind analysis system. *J. Wind Engineer. and Indust. Aerodyn.* 77&78, 53–64.
- Shapiro, L.J., 1983. The asymmetric boundary layer flow under a translating hurricane. *J. Atmos. Sci.* 40, 1984–1998.
- Skamarock, W.C., J.B. Klemp, J. Dudhia, D.O. Gill, D.M. Barker, M.G. Duda, X.-Y. Huang, W. Wang, and J.G. Powers, 2008. A Description of the Advanced Research WRF Version 3. NCAR/TN-475+STR, NCAR Technical Note.
- Smith, T.A., Chen, S., Campbell, T., Rogers, E., Gabersek, S., Wang, D., Carroll, S., Allard, R., 2013. Ocean-wave coupled modeling in COAMPS-TC: a study of Hurricane Ivan (2004). *Ocean Model.* 69, 181–194. doi:10.1016/j.ocemod.2013.06.003.
- Steele, K.E., Teng, C.-C., Wang, D.W.C., 1992. Wave direction measurements using pitch-roll buoys. *Ocean Eng.* 19 (4), 349–375.
- Stopa, J.E., Cheung, K.F., Garces, M.A., Badger, N., 2012. Atmospheric infrasound from nonlinear wave interactions during Hurricanes Felicia and Neki of 2009. *J. Geophys. Res.–Oceans* 117. doi:10.1029/2012JC008257.
- Wallcraft, A.J., E.J. Metzger, and S.N. Carroll, 2009. Software Design Description for the HYbrid Coordinate Ocean Model (HYCOM) Version 2.2. Tech. Rep., NRL/MR/732009-9166.
- Walsh, E.J., Wright, C.W., Vandermark, D., Krabill, W.B., Garcia, A.W., Houston, S.H., Murillo, S.T., Powell, M.D., Black, P.G., Marks Jr., F.D., 2002. Hurricane directional wave spectrum spatial variation at landfall. *J. Phys. Oceanogr.* 32, 1667–1684.
- Wright, C.W., Walsh, E.J., Vandemark, D., Krabill, W.B., Garcia, A.W., Houston, S.H., Powell, M.D., Black, P.G., Marks, F.D., 2001. Hurricane directional wave spectrum spatial variation in the open ocean. *J. Phys. Oceanogr.* 31, 2472–2488.
- Young, I.R., 1994. On the measurement of directional wave spectra. *Appl. Ocean Res.* 16, 283–294.
- Zachry, B.C., Schroeder, J.L., Kennedy, A.B., Westerink, J.J., Letchford, C.W., Hope, M.E., 2013. A case study of nearshore drag coefficient behavior during Hurricane Ike (2008). *J. Appl. Meteorol. Climatol.* 52, 2139–2146.